Electronic properties of the high electron mobility $Al_{0.56}In_{0.44}Sb/Ga_{0.5}In_{0.5}Sb$ heterostructure

L. Desplanque,[1,a)] D. Vignaud,[1] S. Godey,[1] E. Cadio,[1] S. Plissard,[1] X. Wallart,[1] P. Liu,[2] and H. Sellier[2]

[1]*Institut d'Electronique, de Microélectronique et de Nanotechnologie, UMR CNRS 8520, Université des Sciences et Technologies de Lille, Avenue Poincaré, P.O. Box 60069, 59652 Villeneuve d'Ascq Cedex, France*

[2]*Institut Néel, CNRS and Univ. Joseph Fourier, BP 166, 25 av. des Martyrs, F-38042 Grenoble Cedex 9, France*

(Received 22 April 2010; accepted 8 July 2010; published online 17 August 2010)

Electronic properties of the $Al_{0.56}In_{0.44}Sb/Ga_{0.5}In_{0.5}Sb$ heterostructure grown by molecular beam epitaxy are investigated. We measure by means of x-ray photoemission spectroscopy, photoluminescence, and Hall effect measurements the key parameters involved in the achievement of a high speed and very low power consumption field effect transistor: conduction and valence band offsets, energy gaps of channel and barrier materials, electron effective mass, and density of states in the channel. We observe the influence of the quantum well thickness on the electron Hall mobility and sheet carrier density. A type I heterostructure exhibiting a room temperature electron mobility of 25 000 $cm^2\ V^{-1}\ s^{-1}$ with a sheet carrier density of 1.5×10^{12} cm^{-2} is demonstrated for the widest channel. We show that the thickness of the channel influences both Hall density and mobility through a multisubband occupancy. We discuss about the scattering mechanisms limiting the mobility in the second subband. © *2010 American Institute of Physics*. [doi:10.1063/1.3475709]

I. INTRODUCTION

High speed electronic devices for analog applications require large electron mobility materials to work at very low supply voltages.[1] The low electron effective mass needed to reach these low power consumption applications can be obtained using narrow band gap III–V materials. For instance, the theoretical room temperature mobility in InAs or InSb reaches 35 000 $cm^2\ V^{-1}\ s^{-1}$ or 78 000 $cm^2\ V^{-1}\ s^{-1}$, respectively. These values have been experimentally approached using molecular beam epitaxy (MBE).[2–4] However, the unique transport properties of these semiconductors are not sufficient to achieve high speed electronic devices and particularly field effect transistors (FETs). Ideally, a large band gap lattice-matched material should be combined to build a type I heterostructure with a large conduction band offset. These properties are necessary to obtain mesa isolation, a good Schottky gate contact and a high electron mobility with a large sheet carrier density. The type I configuration is essential to avoid hole current leakage from the channel to the gate or an accumulation of holes, generated by impact ionization, in the buffer. In this context, even though InAs and InSb exhibit the best channel conductivity for high speed and low power field effect devices, the combined barrier materials do not show the characteristics mentioned above to benefit from this outstanding transport properties.

For InAs, the natural barrier material is AlSb. Excellent electron transport properties have been demonstrated by Kroemer[2] with the heterostructure. But the achievement of high electron mobility transistors (HEMTs) is strongly limited by its type II configuration, for which there is no confinement of holes in the channel. Another limitation comes from the ~1% mismatch between the two materials which prevents from growing a channel thicker than 15 nm without dislocations.

For InSb, the only possible heterostructure is obtained with an AlInSb barrier. However, due to the intrinsic strained nature of this combination, a drastic trade-off between Al content in the barrier and the InSb channel thickness is imposed, limiting the conduction band offset. This leads to a rapid decrease in the electron mobility while increasing the sheet carrier density. The other negative points concern the poor insulating property of AlInSb with a lower than 30% aluminum content and the difficulty to obtain a good Schottky contact on such a low band gap material. However, AlInSb/InSb HEMTs have been demonstrated by Ashley *et al.*[5] with a record f_T frequency of 305 GHz.

We have proved recently that a high electron mobility heterostructure can be achieved using the $Al_{0.56}In_{0.44}Sb/Ga_{0.5}In_{0.5}Sb$ system.[6] An electron mobility of 18 000 $cm^2\ V^{-1}\ s^{-1}$ with a sheet carrier density of 2.2×10^{12} cm^{-2} has been reported for a Te-doped structure. However, even though some models can predict the band parameters of such structures, particularly the type I configuration, no experimental data exist to validate the calculated band offsets, material band gaps or mobility and density of states (DOS) in $Ga_{0.5}In_{0.5}Sb$. These properties are key parameters for a high speed low power FET. Another interest of this heterostructure is its potential application in the achievement of low power complementary digital circuit.[7]

In this article, we report on the measurement of the valence band offset between $Al_{0.56}In_{0.44}Sb$ and $Ga_{0.5}In_{0.5}Sb$ by x-ray photoelectron spectroscopy (XPS). We obtain from photoluminescence (PL) the band gap energies of AlInSb and

a)Electronic mail: ludovic.desplanque@iemn.univ-lille1.fr.

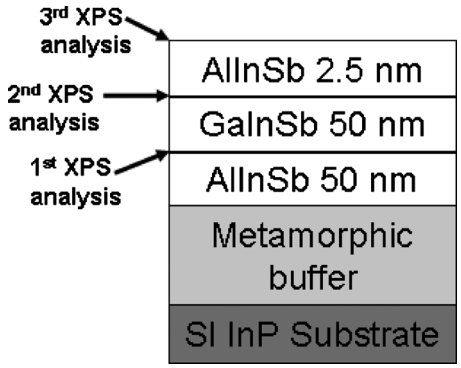

FIG. 1. Schematic cross section of sample A.

GaInSb and deduce the conduction band offset. The electron effective mass is adjusted after PL measurements on thickness-dependent GaInSb quantum wells (QWs). Finally, we report on Te δ-doped heterostructures and discuss about the influence of the QW thickness on the electron mobility and sheet carrier density.

II. EXPERIMENTAL DETAILS

The heterostructures were grown by MBE in a 3 in. RIBER Compact21TM reactor. Standard effusion cells were used to evaporate the group III elements. GaTe was used as n-type dopant source using the same cell temperature for all the n-doped layers. A valved cracker cell was used to produce Sb_2. The fluxes were calibrated using reflexion high energy electron diffraction specular beam intensity oscillations on GaAs, GaSb, and InAs substrates. For all the following samples, a V/III ratio between 2 and 3 was used and the growth rate was about 0.7 monolayers(ML) s^{-1}. The growth was initiated from an InP (001) semi-insulating substrate. The same metamorphic buffer was adopted for all the structures:[6] after the oxide desorption at 550 °C under As pressure, a 100 nm AlInAs layer lattice-matched on InP was grown to smooth the surface; a 400 nm layer of AlSb was then used to accommodate half of the 7.15% lattice mismatch between InP and $Al_{0.56}In_{0.44}Sb$; a 1.2 μm linear graded $Al_{1-x}In_xSb$ buffer with x varying from 10% to 50% was then added before a 10 nm $Al_{1-x}In_xSb$ inverse step to x=44% for optimizing the strain relaxation, finally a 300 nm plateau of $Al_{0.56}In_{0.44}Sb$ was grown to reduce the density of threading dislocations. At the end of the buffer, the temperature was set to 450 °C for the growth of the active part. We kept a constant In flux to avoid any growth interruption at the interfaces between AlInSb and GaInSb.

Various samples were grown for this study. Sample A is used to determine the valence band offset between $Al_{0.56}In_{0.44}Sb$ and $Ga_{0.5}In_{0.5}Sb$ using XPS, according to a commonly used procedure.[8] It consists of a three-step growth (Fig. 1). After the metamorphic buffer and the final $Al_{0.56}In_{0.44}Sb$ plateau, the growth is interrupted; the substrate is cooled down and transferred under ultrahigh vacuum (1×10^{-10} Torr) into the XPS chamber. We use a monochromatic Al $K\alpha$ x-ray source for which the ultimate overall resolution as measured from the full width at half maximum of the Ag $3d_{5/2}$ line is 0.5 eV. According to Fig. 2, we then

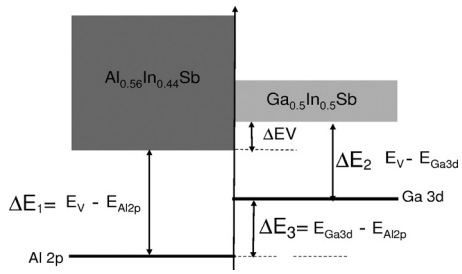

FIG. 2. Schematics of the XPS measurements realized on sample A to extract the valence band offset between AlInSb and GaInSb.

measure $\Delta E_1 = E_V(Al_{0.56}In_{0.44}Sb) - E_{Al\ 2p}(Al_{0.56}In_{0.44}Sb)$. On the same sample, a subsequent growth of 50 nm $Ga_{0.5}In_{0.5}Sb$ is performed and the same method applied to get $\Delta E_2 = E_V(Ga_{0.5}In_{0.5}Sb) - E_{Ga\ 3d}(Ga_{0.5}In_{0.5}Sb)$. Since the electron escape depth is around 3 nm for the considered electron kinetic energies, a 50 nm thickness is sufficient to probe only the $Ga_{0.5}In_{0.5}Sb$ layer without any influence of the underlying $Al_{0.56}In_{0.44}Sb$ buffer. Finally, a 2.5-nm-thick $Al_{0.56}In_{0.44}Sb$ layer is grown on top of the 50 nm GaInSb one, on which we extract $\Delta E_3 = E_{Ga\ 3d} - E_{Al\ 2p}$. In this case, the 2.5 nm thickness is chosen to be sensitive to both the surface $Al_{0.56}In_{0.44}Sb$ and the underlying $Ga_{0.5}In_{0.5}Sb$ layers. According to Fig. 2, the valence band offset ΔE_V is then obtained by: $\Delta E_V = \Delta E_3 + \Delta E_2 - \Delta E_1$.

Samples B and C are two stacks of undoped AlInSb/GaInSb/AlInSb QWs of different thickness. The sample B is depicted on Fig. 3. It consists of two GaInSb QW (50 nm and 9 nm, respectively) separated by a 200 nm AlInSb barrier. The top barrier is 100 nm thick and the structure is capped with a 5 nm GaInSb layer. The stack of sample C is displayed on Fig. 4. It is composed of three GaInSb QW with a thickness of 12 nm, 6 nm, and 4 nm, respectively (from the bottom to the top). The QW are separated with 200-nm-thick AlInSb barriers. The same barrier separates the top QW from a 4 nm GaInSb cap layer. Samples D, E, and F consist of tellurium δ-doped heterostructures with different GaInSb channel thicknesses (10 nm, 15 nm, and 25 nm, respectively). After the channel growth, these samples consist of a

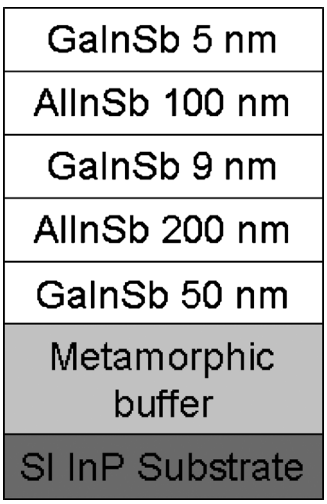

FIG. 3. Schematic cross section of sample B.

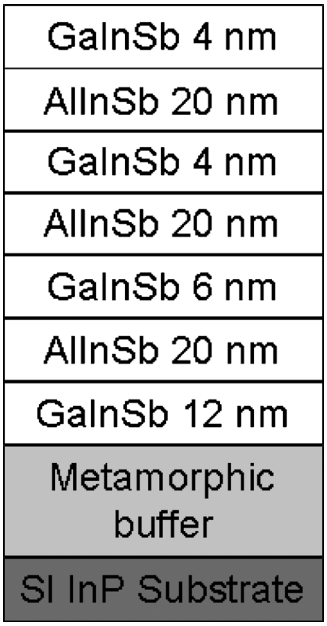

FIG. 4. Schematic cross section of sample C.

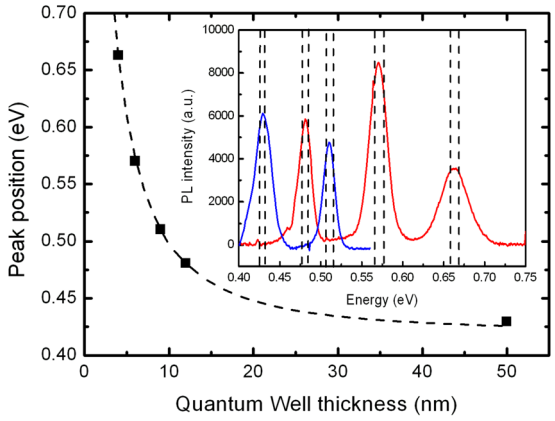

FIG. 6. (Color online) Position of PL peaks vs AlInSb/GaInSb QW thickness extracted from the PL spectra displayed on the inset and measured on sample B (first and third peaks from the left) and C (second, fourth, and fifth peaks from the left). The theoretical value of the E_1-HH_1 transition calculated using an electron effective mass of 0.023 m_0 is superimposed. The vertical dashed lines in the inset correspond to the theoretical position of the different peaks using an electron effective mass either of 0.019 m_0 (line on the right of the peaks) or 0.0265 m_0 (line on the left of the peaks).

5 nm AlInSb spacer, a Te δ-doping plane inserted between 4 ML of AlSb, a 10 nm AlInSb barrier, and a Te-doped GaInSb cap layer (Fig. 5).

All the samples (except for A) were characterized by 10 K PL using an InSb detector cooled at 77 K. For samples D, E, and F, we also performed Hall Effect measurements using the van der Pauw configuration with ohmic contacts obtained by alloying indium through the top barrier at 200 °C for 10 min. Eventually, magnetotransport measurements were carried out at 4 K on sample F to evaluate the multisubband occupancy for electrons in the channel.

III. RESULTS

The values of discontinuities denoted as ΔE_1, ΔE_2, and ΔE_3 on Fig. 2 are deduced from the XPS spectra analyses. We obtain, respectively, 73.25 ± 0.02 eV, 18.94 ± 0.02 eV, and 54.52 ± 0.02 eV. Thus, the valence band offset between the two materials is determined as 0.21 ± 0.05 eV at room temperature. Since the bandgaps of $Al_{0.56}In_{0.44}Sb$ and $Ga_{0.5}In_{0.5}Sb$ are expected to show a similar temperature dependency (about +70 meV from 300 to 10 K according to Vurgaftman *et al.*[11]), this valence band offset can be considered as still valid at 10 K.

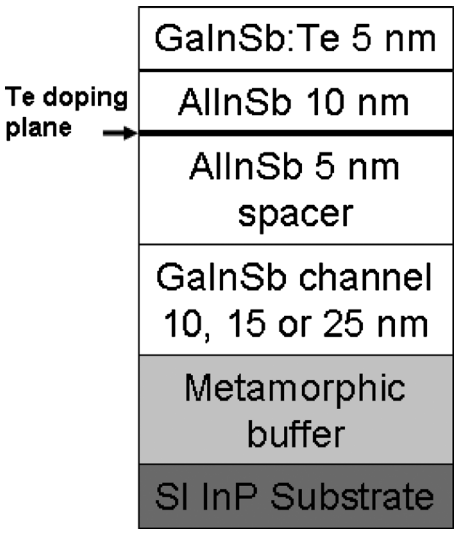

FIG. 5. Schematic cross sections of samples D, E, and F with channel thicknesses of 10 nm, 15 nm, and 25 nm, respectively.

PL spectra measured at 10 K on samples B and C are displayed in the inset of Fig. 6. For each sample, we can identify the QW thickness-dependent peak corresponding to the main optical transition (labeled E_1-HH_1). Another part of the spectra, not shown on the inset of Fig. 6, reveals a peak at 1.29 eV, attributed to electron–hole recombinations revealing the bandgap of the AlInSb barrier. The band gap energy of $Ga_{0.5}In_{0.5}Sb$ (0.43 eV) is directly deduced from the PL measurement in the thickest QW (50 nm), for which confinement effects on electrons and holes can be neglected. The measurement of $Al_{0.56}In_{0.44}Sb$ and $Ga_{0.5}In_{0.5}Sb$ band gaps, associated with the evaluation of the ΔE_V value obtained by the XPS analysis, leads to a full determination of the band parameters for the $Al_{0.56}In_{0.44}Sb/Ga_{0.5}In_{0.5}Sb$ heterostructure. The type I configuration of the structure is confirmed and a conduction band offset of 0.65 eV $\pm$ 0.05 eV between the two materials is deduced.

Assuming such band parameters, we used a model based on the Schrödinger equation solution to check the effective mass value of electrons in $Ga_{0.5}In_{0.5}Sb$. For $m_e^\star = 0.023 \pm 0.004$ m_0, which is almost the same electron effective mass as in InAs, we observe a very good agreement between the position of the PL peaks and the calculated curve (Fig. 6). As an estimation of the uncertainty of this effective mass deduction, we added on the inset of Fig. 6 vertical dashed lines corresponding to the peak position calculation using an electron effective of 0.019 or 0.0265 m_0.

The result of van der Pauw measurements obtained at 300 and 77 K on the samples D, E, and F are plotted in Fig. 7. The measured electron sheet density is almost constant for

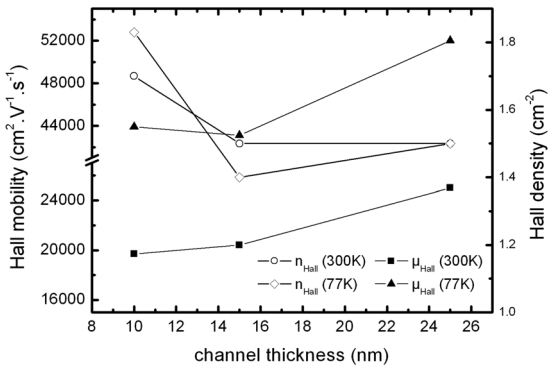

FIG. 7. Hall mobilities and sheet electron densities vs channel thickness deduced from van der Pauw measurements on sample D (10 nm), sample E (15 nm), and sample F (25 nm).

the samples with 15 or 25 nm channel (about 1.5×10^{12} cm^{-2}) whereas a slightly larger value is obtained for the 10 nm channel sample (about 1.8×10^{12} cm^{-2}). We observe an increase in the Hall mobility for the widest channel with a maximum room temperature value of 25 000 cm^2 V^{-1} s^{-1}.

The occupancy of confined electronic levels in the conduction band of a δ-doped GaInSb QW was investigated by PL experiments. The injection of photogenerated holes in the QW induces radiative recombinations with electrons of the Fermi sea revealing the singularities of the conduction band and particularly the ground energies of the populated subbands.[9,10]

The spectra measured on samples D, E and F are displayed in Fig. 8. Unfortunately, the energy region of interest is partly hidden or deformed by carbon dioxide absorption (between 0.43 and 0.49 eV), resulting in some parasitic peaks in this range (mainly at 0.459 and 0.469 eV). A 488 nm photon flux of about 6×10^{21} photons cm^{-2} s^{-1} has been used.

For the thinnest QW heterostructure [see Fig. 8(a)], one peak is observed with an extending tail toward high energies. This peak is attributed to the E_1-HH_1 transition. The high energy tail extending up to 0.65 eV is due to the recombinations of hot electrons up to the Fermi level with heavy holes from the ground valence band level. This result is consistent with the electron DOS of about 1×10^{13} cm^{-2} eV^{-1}, deduced from the electron effective mass of 0.023 m_0 using the formula $DOS = m^*/(\pi\hbar^2)$ (where $\hbar$ is the reduced Planck's constant). Indeed, this value of DOS would induce a spreading of electrons on the range of 180 meV for the 1.8×10^{12} cm^{-2} electron density measured by Hall effect.

For the 15 nm QW heterostructure [see Fig. 8(b)], the shape of the PL spectra is quite different. Indeed, it exhibits multiple maxima with a dominant peak at high energy (about 0.54 eV). This peak is attributed to the E_2-HH_1 transition. The lower confinement of electrons in this wider well induces a decrease in the second conduction subband ground energy below the Fermi level.

For the 25 nm QW heterostructure [see Fig. 8(c)], PL is observed from about 0.44 to 0.52 eV. In the latter, the low confinement of electrons leads to very close E_1-HH_1 and E_2-HH_1 transitions. In addition to the perturbation induced

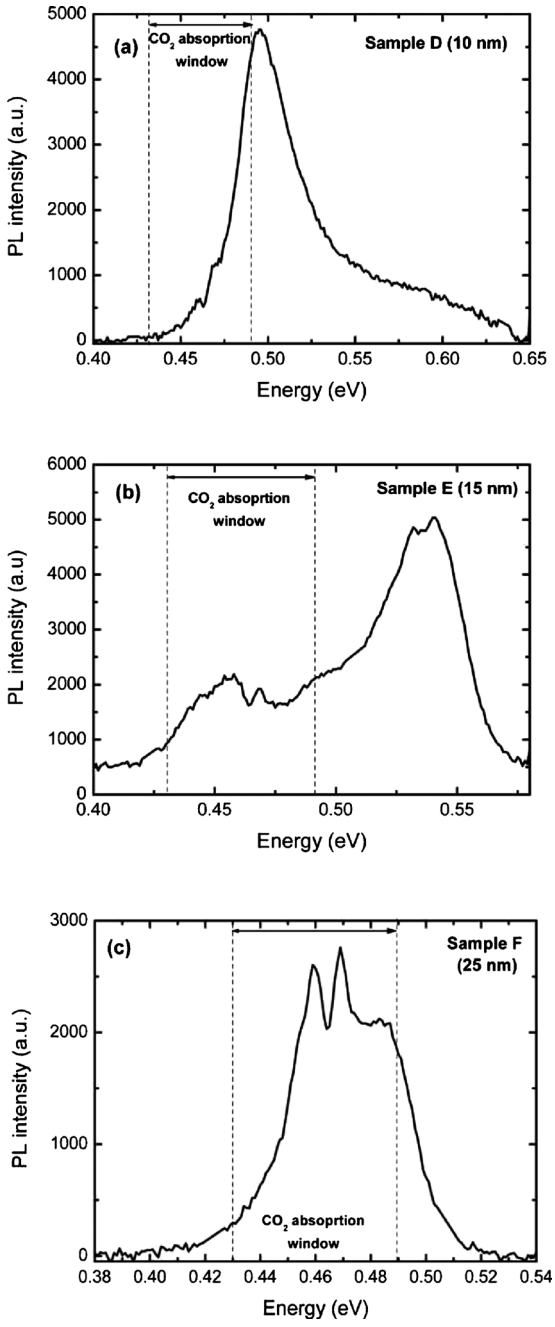

FIG. 8. 10 K PL measurements on the δ-doped heterostructures D (a), E (b), and F (c) for an optical excitation power of 25 $\mu W/\mu m^2$ (the CO_2 absorption window is delimited by the two vertical dashed lines).

by CO_2 absorption in this range of energy, this causes some difficulties to clearly distinguish two separate peaks in the PL spectrum but two conduction subbands are probably occupied.

To evaluate the occupancy rate of the second electron subband in this sample, we have performed magnetotransport measurements at 4 K. The measured in-plane resistivities are displayed in Fig. 9. From these results, we perform an analysis assuming that the two-dimensional resistivity coefficients (assuming no Landau level formation) are given by:[13]

$$\rho_{xx} = (D_1 + D_2)/[(D_1 + D_2)^2 + (A_1 + A_2)^2], \quad (1)$$

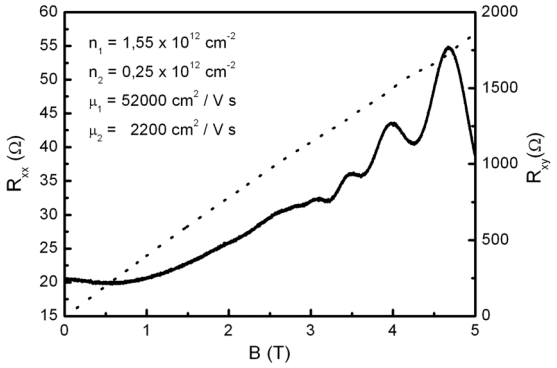

FIG. 9. Magnetotransport measurement at 4 K on sample F: solid line is the R_{xx} resistivity and dashed line is the R_{xy} resistivity.

$$\rho_{xy} = (A_1 + A_2)/[(D_1 + D_2)^2 + (A_1 + A_2)^2], \quad (2)$$

where D_i and A_i ($i=1$ or 2) are two sets of parameters for the two subbands given by:

$$D_i = en_i\mu_i/[1 + (\mu_i B)^2], \quad (3)$$

$$A_i = en_i\mu_i^2 B/[1 + (\mu_i B)^2], \quad (4)$$

where e is the electron charge, n_i and μ_i the electron sheet density and mobility on the first subband and B the applied magnetic field.

This model predicts an increase in ρ_{xx} and a decrease in the ρ_{xy} slope versus field, as compared with the single subband model. It is indeed the case (see Fig. 9). The experimental results are fitted by adjusting D_i and A_i parameters, their respective values being summarized in Fig. 9.

IV. DISCUSSION

Two scattering mechanisms can contribute to the increasing Hall mobility with the channel thickness observed at 300 and 77 K. For such a thin spacer heterostructure (5 nm), scattering by remote donor impurities is important. As the channel thickness increases, the maximum of the wave function of electrons is displaced away from the upper interface of the QW, reducing the interactions of electrons with remote donor impurities. As demonstrated by Bolognesi *et al.*,[12] interface roughness scattering can also be significant at room temperature for thin QW on a metamorphic buffer. We measured by atomic force microscopy a root mean square roughness of about 5 nm on a 25 μm^2 image [the surface exhibits height fluctuations of about 8 nm on a lateral scale of about 500 nm (Ref. 6)].

Considering the results of the magnetotransport measurements on sample F, the first observation is that the sum of the two subband densities is almost the same as the Hall density measured on sample D where only one subband is occupied (about 1.8×10^{12} cm^{-2}). It is consistent with the same amount of Te incorporated in the doping plane. This result indicates that the Hall density measured on wide channel heterostructure underestimates the total sheet carrier density in the QW (the same value of about 1.5×10^{12} cm^{-2} was obtained at 77 and 10 K). This underestimation is due to the outstanding low mobility of electrons in the second subband as revealed by the magnetotransport measurements analysis (about twenty times lower). Indeed, in a two level system, the relationship between Hall density and sheet carrier densities and mobilities in the two subbands that can be deduced from the expression of the ρ_{xy} coefficient at low magnetic field is given by:

$$n_H = [(n_1\mu_1 + n_2\mu_2)^2]/(n_1\mu_1^2 + n_2\mu_2^2), \quad (5)$$

where n_H is the Hall electron density and n_i and μ_i are, respectively, the density and mobility of electrons occupying the ith subband. When the mobility and density of carriers in the second subband are low, they do not significantly change the conductivity of the channel and the measured Hall value correspond to the sheet density in the first subband. Similarly but to a lesser extent, the reduction in Hall electron mobility induced by the second subband occupancy has been reported for other systems such as AlSb/InAs (Refs. 14 and 15) or AlGaAs/GaAs heterostructures.[16] In the latter paper, the mobility of electrons in each subband is extracted from the magnetotransport measurement using a standard classical model and the authors attribute the low electron mobility in the second subband to a smaller value of the Fermi velocity in the second subband due to the reduced sheet concentration of electrons. This implies a more effective ionized impurity scattering for the slowly moving electrons in the second subband. Another consequence of the larger Fermi wavelength $\{\lambda_F=[(2\pi/n)^{1/2}]\}$ is the increase in the effectiveness of other scattering mechanisms such as interface roughness, alloy disorder, background impurities, or dislocations.

V. CONCLUSION

We have measured the electronic properties of the $Al_{0.56}In_{0.44}Sb/Ga_{0.5}In_{0.5}Sb$ heterostructure. A type I configuration with a large conduction band offset of 0.65 eV and an electron effective mass of 0.023 m_0 have been demonstrated. Electron transport properties in modulation doped heterostructures have been investigated at room temperature and 77 K. The highest room temperature electron mobility, 25 000 $cm^2\ V^{-1}\ s^{-1}$, was achieved for the widest channel (25 nm). This result is attributed to a decrease in both interface roughness scattering and remote donor impurity scattering for samples with a wide channel. PL measurements correlated with magnetotransport experiments at 4 K revealed the occupancy of a second subband in this case with a seriously degraded electron mobility on the second level. This phenomenon is probably related to the low sheet electron density in the second subband leading to an increase in the Fermi wavelength of electron and thus of the scattering mechanisms. The occupation of a second subband with a low electron mobility leads to an underestimation of the total sheet carrier density by Hall measurement. These results suggest that the heterostructure could be further improved by an enhancement of the metamorphic buffer to reduce both the threading dislocation density and the surface roughness. However, the demonstrated electronic properties with a wide channel are very promising for the realization of high speed and very low power consumption field effect devices.

ACKNOWLEDGMENTS

We would like to thank J.-L. Codron for his help in preparation and growth of the samples. This work has been achieved with the financial support of the European Union, the French Government within the MOS35 and MICATEC ANR projects and the Regional Council.

[1]G. Dambrine, S. Bollaert, Y. Roelens, A. Noudeviwa, F. Danneville, A. Olivier, N. Wichmann, L. Desplanque, X. Wallart, J. Grahn, G. Moschetti, P. A. Nilsson, M. Malmkvist, and E. Lefebvre, *67th Device Research Conference*, 22–24 June (State College, PA, USA, 2009), pp. 149–151.
[2]H. Kroemer, Physica E (Amsterdam) **20**, 196 (2004).
[3]L. Desplanque, D. Vignaud, and X. Wallart, J. Cryst. Growth **301–302**, 194 (2007).
[4]J. M. S. Orr, A. M. Gilbertson, M. Fearn, O. W. Croad, C. J. Storey, L. Buckle, M. T. Emeny, P. D. Buckle, and T. Ashley, Phys. Rev. B **77**, 165334 (2008).
[5]T. Ashley, L. Buckle, S. Datta, M. T. Emeny, D. G. Hayes, K. P. Hilton, R. Jefferies, T. Martin, T. J. Phillips, D. J. Wallis, P. J. Wilding, and R. Cahu, Electron. Lett. **43**, 777 (2007).
[6]G. Delhaye, L. Desplanque, and X. Wallart, J. Appl. Phys. **104**, 066105 (2008).
[7]B. R. Bennett, M. G. Ancona, J. G. Champlain, N. A. Papanicolaou, and J. B. Boos, J. Cryst. Growth **312**, 37 (2009).
[8]O. Dehaese, X. Wallart, O. Schuler, and F. Mollot, J. Appl. Phys. **84**, 2127 (1998).
[9]H. Brugger, H. Müssig, C. Wölk, K. Kern, and D. Heitmann, Appl. Phys. Lett. **59**, 2739 (1991).
[10]T. W. Kim, M. Jung, and D. U. Lee, Appl. Surf. Sci. **93**, 131 (1996).
[11]I. Vurgaftman, J. R. Meyer, and L. R. Ram-Mohan, J. Appl. Phys. **89**, 5815 (2001).
[12]C. Bolognesi, H. Kroemer, and J. H. English, Appl. Phys. Lett. **61**, 213 (1992).
[13]M. van der Burgt, V. C. Karavolas, F. M. Peeters, J. Singleton, R. J. Nicholas, F. Herlach, J. J. Harris, M. Van Hove, and G. Borghs, Phys. Rev. B **52**, 12218 (1995).
[14]S. Sasa, Y. Yanamoto, S. Izumiya, M. Yano, Y. Iwai, and M. Inoue, Jpn. J. Appl. Phys., Part 1 **36**, 1869 (1997).
[15]B. R. Bennett, M. J. Yang, B. V. Shanabrook, J. B. Boos, and D. Park, Appl. Phys. Lett. **72**, 1193 (1998).
[16]H. van Houten, J. G. Williamson, and M. E. I. Broekaart, Phys. Rev. B **37**, 2756 (1988).